Physical Insights into Chemistry, Catalysis, and Interfaces

Electrochemically Generated Nanobubbles: Invariance of the Current with Respect to Electrode Size and Potential

Esteban D. Gadea, Yamila A. Perez Sirkin, Valeria Molinero, and Damian A. Scherlis

J. Phys. Chem. Lett., **Just Accepted Manuscript** • DOI: 10.1021/acs.jpclett.0c01404 • Publication Date (Web): 21 Jul 2020

Electrochemically Generated Nanobubbles: Invariance of the Current with Respect to Electrode Size and Potential

Esteban D. Gadea,[†] Yamila A. Perez Sirkin,[†] Valeria Molinero,[‡*] and Damian A. Scherlis[†*]

[†] Departamento de Química Inorgánica, Analítica y Química Física/INQUIMAE, Facultad de Ciencias Exactas y Naturales, Universidad de Buenos Aires, Ciudad Universitaria, Pab. II, Buenos Aires, C1428EHA, Argentina.

[‡]Department of Chemistry, The University of Utah, 315 South 1400 East, Salt Lake City, Utah 84112-0850, United States.

Email: damian@qi.fcen.uba.ar; valeria.molinero@utah.edu

ABSTRACT. Gas-producing electrochemical reactions are key to energy conversion and generation technologies. Bubble formation dramatically decreases gas-production rates on nanoelectrodes, by confining the reaction to the electrode boundary. This results in the collapse of the current to a stationary value independent of the potential. Startlingly, these residual currents also appear to be insensitive to nanoelectrode diameter in the 5 to 500 nm range. These results are counterintuitive, as it may be expected that the current be proportional to the circumference of the electrode, *i.e.* the length of the three-phase line where the reaction occurs. Here we use molecular simulations and a kinetic model to elucidate the origin of current insensitivity with respect to the potential and establish its relationship to the size of nanoelectrodes. We provide critical insights for the design and operation of nanoscale electrochemical devices and demonstrate nanoelectrode arrays maximize conversion rates compared to macroscopic electrodes of same total area.

TOC FIGURE

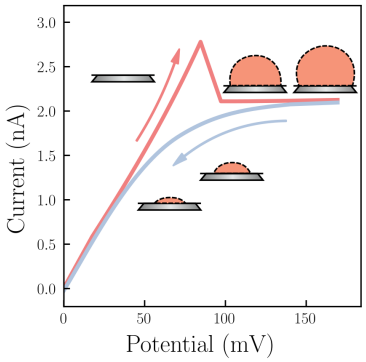

Gas evolution reactions are at the core of electrochemical technologies for energy conversion and storage.[1-6] Processes like water splitting, hydrogen evolution, CO_2 reduction for fuel regeneration, and CO_2 production in fuel cells, typically generate gas bubbles attached to the catalysts.[7-9] These bubbles decrease the mass transfer dynamics and conductance, raising the ohmic drop during the reaction.[1, 10-15] The growing thrust towards using nanoparticles as catalysts in gas evolving reactions[16-21] makes understanding the effect of surface nanobubbles on reaction rates paramount,[1, 22] but whether and how the use of nanoelectrodes affects the efficiency of gas-formation reactions are still open questions.

Experiments with nanoelectrodes showed that single nanobubbles are formed on individual disks as large as 90 nm.[1, 23-34] In principle many bubbles might nucleate on one nanoelectrode but, due to coalescence and Ostwald ripening, the system evolves towards a stationary state with single bubbles covering individual nanoelectrodes.[22] Bubble nucleation is associated with a sharp drop of the current to a residual value i_r above a threshold potential.[23-24] The nanobubble attains a stationary state through compensation between the diffusive outflux of gas at the bubble-solution interface and its electrochemical production on the three-phase electrode-bubble-solution line.[23, 29, 35-36] Experiments report that the residual current in the stationary regime does not depend on the applied voltage.[23-28] On this basis, it has been previously assumed that the size and shape of the stationary nanobubbles are invariant with applied potential.[29, 35] We recently reproduced the experimental currents, stages, and critical nucleus size in the formation of nanobubbles using molecular simulations combined with a simple scheme to model the electrochemical gas generation.[36] Our study revealed that the size of the stationary nanobubble and its contact angle changed with the reaction driving force, despite invariability of the residual current. This unexpected finding unveiled the existence of a myriad of stationary states with different sizes, shapes, and internal pressures, associated with the same current.[36]

The residual currents i_r are not just independent of the potential, but also appear to be quite insensitive to nanoelectrode diameter in the 5 to 500 nm range investigated through experiments.[23-25, 35] These results are counterintuitive, as it may be expected that the current be proportional to the circumference of the electrode, *i.e.* the length of the three-phase line where the reaction occurs. Elucidating the origin of the insensitivity of the residual current to the potential and establishing its relationship to the size of the nanoelectrode, are the goals of this study.

We perform molecular dynamics simulations using a modified version of the model of gas evolution on a single nanoelectrode developed in ref. [36] (Illustration 1 and Supp. Info. A): a Pt disk electrode is embedded in a crystalline inert wall and in contact with water, modeled with the mW model.[37] The nature of the intermolecular interactions and the adopted parameters are discussed in Supp. Info. A. The chemical reaction reversibly converts a water molecule into gas using a kinetic Monte-Carlo algorithm that explicitly accounts for the applied potential bias ΔE (see Supp. Info. A). We compute the currents, geometries, diffusion and dissolution rates of stationary bubbles on planar disk electrodes of diameter 3, 5, 7 and 9 nm as a function of the electrode size and applied potential, assuming a one-electron reaction, Solvent → Gas + 1 e^-. In what follows we show that—in agreement with the experiments[23-26]—the simulations predict that the current is insensitive to the potential and size of the nanoelectrode. We demonstrate that this insensitivity is a consequence of the compensation between the decrease in the area of the bubble exposed to the solvent and the increase in its Laplace pressure with the size of the bubble. We further establish the range of electrode sizes and potentials for which these results are valid, and make quantitative predictions on the onset of electrode sizes for which deviations from such invariants should be observed in experiments.

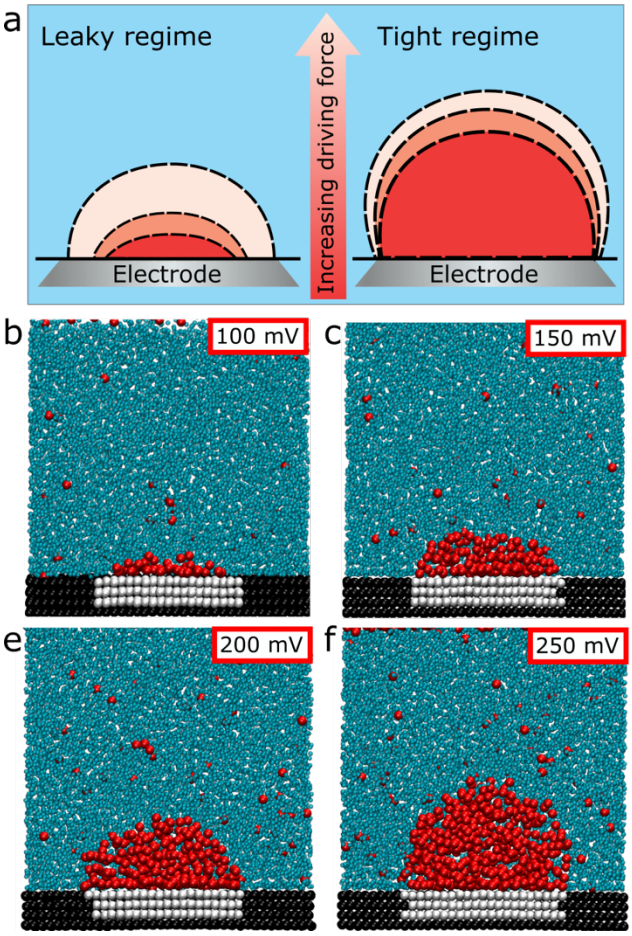

Illustration 1. Size and shape of electrochemically-generated pinned nanobubbles depends on the applied potential. (a) Illustration of the evolution of stationary pinned nanobubbles with electrode potential in the leaky and tight regimes. (b-f) Representative cross-sectional snapshots from simulations of

the stationary bubbles, showing how their size and geometry change for potential ΔE between 100 mV and 250 mV for an electrode of 5 nm diameter. Water molecules are represented in blue, gas molecules in red, particles belonging to the electrode in white and particles of the inert wall in black.

Figure 1 shows the simulated voltammetric response for a 7 nm electrode. Starting from a bare electrode, the current initially increases as a function of the potential according to the Buttler-Volmer relation. There is not yet a bubble on the electrode in this regime, and gas molecules produced at the electrode-solution interface diffuse through the solution, establishing a gas concentration profile (shown in Figure S2 of the Supp. Info.). The current increases with a further rise of the potential, until the critical gas concentration needed to nucleate a bubble at the electrode is reached at ΔE around 100 mV. A lower limit of this critical gas concentration can be estimated: the molar fraction of gas on the electrode at 75 mV, just below the potential necessary to nucleate the nanobubble is two orders of magnitude higher than the equilibrium solubility of gas in the model, 0.04 (Supp. Fig. S1). The degree of supersaturation required for bubble nucleation in the simulations, as well as the size of the critical nuclei,[36] are in excellent agreement with those deduced from experiments.[26,] The spike in the forward sweep current (red curve in Figure 1) reflects the fact that the nucleation of the bubble is an activated process that requires overpotential. The growth of the surface bubble blocks the electrode, dropping the current to a small stationary value. The increase in the potential leads to growth of the nanobubble (Illustration 1 and Supp. Fig. S3 for a 5 nm diameter electrode) with a negligible increase in the residual current (Figures 1 and 2a). The evolution of the current upon forward and backward scanning of the potential is in agreement with experiments.[23-32] The correspondence between each feature of the voltammograms in experiments[23-32] and simulations validates our modeling approach, while providing key information on the electrochemically-driven formation of bubbles with molecular resolution unattainable through state of the art experimental measurements.

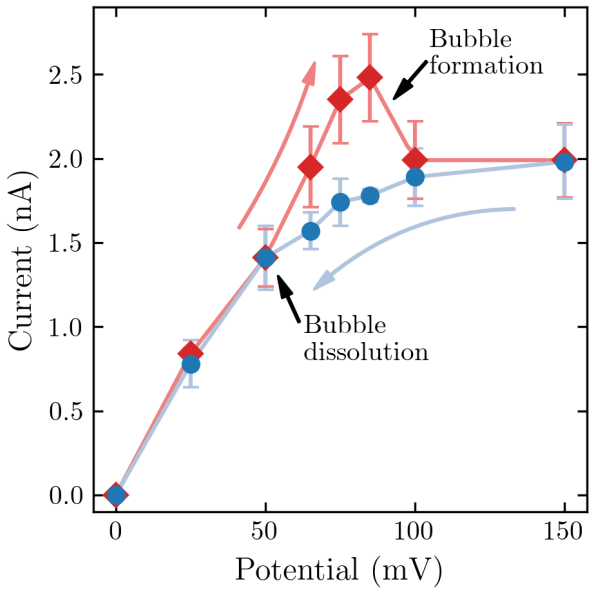

Figure 1. Voltammogram obtained from molecular simulations of gas evolution on a 7 nm diameter electrode. Red diamonds and blue points correspond to the currents registered in the forward and the backward sweep, respectively. The peak in the forward sweep corresponds to the metastable region where the gas is supersaturated at the electrode surface, but the bubble has not yet formed. The backward sweep transits through equilibrium states; the dissolution of the bubble is gradual on decreasing the applied potential.

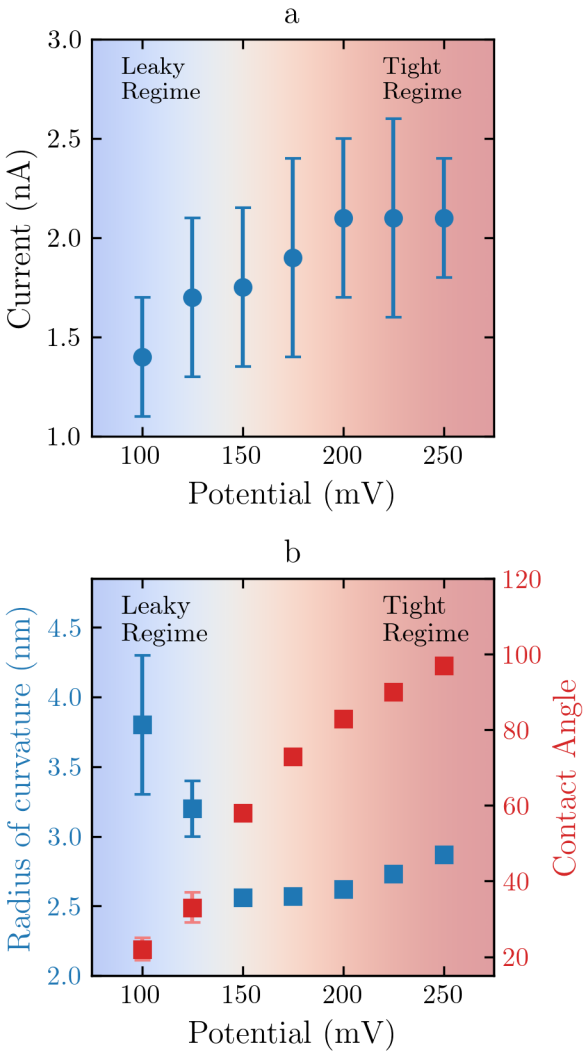

Figure 2: (a) Stationary state currents as a function of the applied potential, on a 5 nm electrode during the backward sweep. (b) Radii of curvature and contact angles for nanobubbles in stationary states as a function of the applied potential. Curvature and contact angles are estimated from the density profiles obtained from time-averaged isosurfaces of the gas distribution (density profiles are shown in Figure S3 of the SI). The plotted values and their error bars correspond to block averages and standard deviations computed every 5 ns over a total of 40 ns for each potential.

The drop of the current to a residual value after the nucleation of the bubble (Figure 1) necessitates that the bubble be pinned to the electrode. The source of the pinning is the difference in wetting properties between the electrode and the inert support that surrounds it.[36] An electrode more hydrophobic than the inert support keeps the bubble in place, evolving the contact angle as the bubble grows. Instead, if the interactions of the gas with the electrode are the same as those with the inert support, the bubble grows with constant contact angle, wandering in and out of the electrode, without ever reaching a stationary state (Illustration 2 and Movie S1). We predict that experiments in which the electrodes and support material have similar hydrophobicity will be unable to pin the bubble, and will not result in stationary currents after bubble formation.

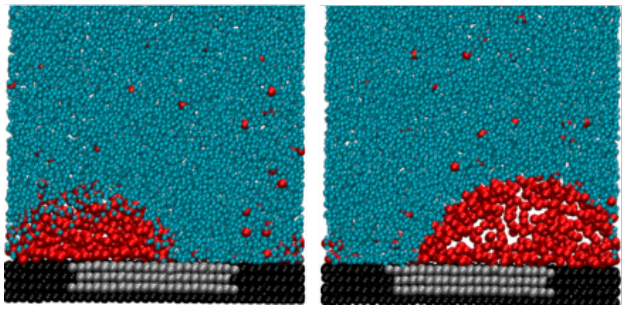

Illustration 2. Snapshots of the simulation of an unpinned nanobubble on a 5 nm diameter electrode at ΔE = 200 mV. Parameters for the interaction potentials between water and the support wall are modified to be equal to the water-electrode potential (electrode interactions remain unchanged, original values are listed in Table S1).

The evolution of the size and shape of pinned stationary nanobubbles as a function of the applied potential cannot yet be obtained from experiments. We characterize the shape of nanobubbles through their contact angle θ with the electrode (measured from inside the bubble) and their radius of curvature R (Figure S3 of the SI). Figure 2 displays the evolution of the current and of these two geometrical parameters with respect to the potential for a stationary bubble on a 5 nm diameter electrode. The average contact angle displays a smooth transition between the value expected for the hydrophobic electrode to a higher one that arises from increasing exposure of the nanobubble to the boundary of the electrode with the hydrophilic surrounding substrate. The radius of curvature of the bubble displays a non-monotonic dependence with the voltage (Figure 2b). When the bubble is smaller than the electrode, R decreases and θ increases with ΔE. Under these conditions, only a fraction of the gas produced is injected into the bubble; the rest leaks directly into the solution. We call this the *leaky* regime (left panel of Illustration 1a). A different trend is observed in Figure 2 at higher potentials: the drop in the radius of curvature ceases and even reverts as the base of the bubble expands to cover the electrode. Although the base of the bubble seems to completely block the electrode in this regime, fluctuations in shape and density near the three-phase electrode-bubble-solution line enable reactant contact with the electrode.[36] All gas molecules produced at the three-phase line in this regime enter the bubble, from where they eventually reach the solution by diffusing out through the gas-liquid interface. We call this the *tight* regime (right panel of Illustration 1a). The growth of the bubble in the *leaky* regime resembles that of an emerging spherical cap with a decreasing radius of curvature, whereas in the *tight* regime the bubble fully covers the surface of the electrode and slightly increases its radius of curvature. Thus, the voltage that minimizes the radius of curvature in Figure

2b coincides with the transition between the *leaky* and *tight* regimes. Below we demonstrate that in the *tight* regime the stationary current is insensitive to the potential and size of the electrode.

Every gas molecule generated at the electrode in the *tight* regime is incorporated to the bubble. Hence, the amount of gas produced, and therefore the current, must be equal to the gas outflux through the bubble surface. The invariance in the current with the potential and size in the tight regime (Fig. 3a) requires that nanobubbles of different sizes and shapes have the same diffusive gas outflux. Integration of the diffusion equation for the spherical cap geometry, as previously done by Lohse and coworkers,[38] yields an expression for the flux of gas through the gas-liquid interface of the bubble. In the quasistatic limit, this quantity turns out to be

$$\frac{dW}{dt} = -\pi D R (C_R - C_\infty) f(\theta), \qquad (1)$$

where W is the mass of gas in the bubble, t the time, D the diffusion coefficient for the gas in solution, C_R and C_∞ the concentrations of gas in solution at the bubble surface and in the bulk, respectively, and $f(\theta)$ a geometrical factor determined by the contact angle and shown in Figure S5 of the SI. The function $f(\theta)$ contains the only dependence of the stationary current of the tight regime on the electrochemical potential. As $f(\theta)$ is a slowly increasing function of the contact angle of the bubble, the small stationary current seems to be independent of the driving force.

To understand the origin of the puzzling insensitivity of the stationary current to the size of the electrode, we explicitly consider the R dependence of the terms in eq. 1. We assume that the concentration C_R at the surface of the bubble is controlled by Henry's Law, $C_R = K_H P$, where the total pressure P of gas in the bubble is the sum of the external pressure, P_{ext}, and the Laplace pressure, $P_{Laplace} = 2\sigma/R$, with σ the surface tension of the bubble-solution interface. We use the Young-Laplace equation for the estimation of the internal pressure of the nanobubble, as this relation has been proven to hold down to the nanometer scale.[39] For diameters below a few tens of nanometers, a typical external gas pressure of 1 bar would be much smaller than the Laplace pressure predicted by the Young-Laplace equation ($P_{ext} << P_{Laplace}$), and P_{ext} can be safely neglected. Assuming that the gas concentration in the bulk, C_∞, is negligible compared to its concentration at the interface, C_R, the total mass diffusive outflux becomes

$$\frac{dW}{dt} = -2\pi D \sigma K_H f(\theta) \qquad (2)$$

and, the flux dW/dt becomes independent of the radius R of the nanobubble. This invariance of the flux with R is a consequence of two opposing effects that arise from bubble miniaturization: the rise in the Laplace pressure due to curvature, and the decrease of the exposed bubble area. The reduction in area has a detrimental effect on the gas outflow, while the higher curvature increases the internal pressure and raises the escape of gas molecules per unit area. These two effects cancel out almost exactly to keep the current invariant with respect to nanobubble size.

We note that equation 1 reproduces equations 6 and 7 of ref. 38. Here this expression has been adapted to the case in which the influx of gas arises from the electrochemical reaction. In the present conditions we neglect C_∞ to arrive to equation 2. Instead, in ref. 38 the interest is on the effect of concentration of gas in the solution on the stability and dynamics of pinned surface nanobubbles, and C_∞ is precisely responsible for the gas influx. In particular, Zhang, Lohse, and co-authors, have characterized nanobubbles in an oversaturated liquid phase.[40-42] At variance with those studies, in our simulations the liquid is in contact with a very low pressure gas phase, and a gradient is established that makes equation 2 effectively independent of C_∞. This is not the case in the models of refs. 40, 41 and 42, where nanobubble stabilization is determined by the oversaturation of the liquid.

Larger sizes of nanoelectrodes can support larger stationary bubbles, for which the assumption of $P_{ext} << P_{Laplace}$ is not valid. Removing this assumption, we predict a slow increase in stationary current for larger electrodes (Figure 3a). The contribution of the external pressure to the total P can be neglected with less than 1% error in the current for electrodes with diameter below ~30 nm. Only when the diameter of the electrode reaches ~2 μm, the stationary current is twice the current of a 3 nm diameter nanoelectrode, which has an area half a million times smaller. We conclude that the use of large arrays of small nanoelectrodes provides a competitive advantage over larger single electrodes of same total area for attaining high overall rates of electrochemical reactions that produce low solubility gases.

Equation 2 demands that nanoelectrodes of different size yield similar residual currents, provided that they have single nanobubbles with comparable contact angles. The molecular simulations validate this prediction: the steady state residual currents for electrodes with diameters 3 to 9 nm at a potential ΔE = 200 mV is insensitive to the length of the three-phase contact (Figure 3b). The slightly lower i_r, for the 3 nm electrode is consistent with the smaller contact angle of the bubble it supports (Figure 3c and Supp. Fig. S5). The currents in Figure 3b follow the same trend as the contact angles in Figure 3c, as expected from equation 2. Figure 3c shows that stationary nanobubbles on different size electrodes at the same electrochemical potential have different geometries. The dependence of the contact angle with diameter cannot be easily anticipated for nanoscale bubbles. Bigger electrodes produce bubbles with less curvature; as a consequence the

internal pressure decreases, leading to decreasing densities that alter the surface energies at the corresponding interfaces. Thus, the shape of the nanobubble would be a very complex function involving five surface tensions: electrode-gas, electrode-solution, support-gas, support-solution and gas-solution. However, the larger the electrode, the slower the variation of the contact angle θ, contributing to the independence of the current to electrode size.

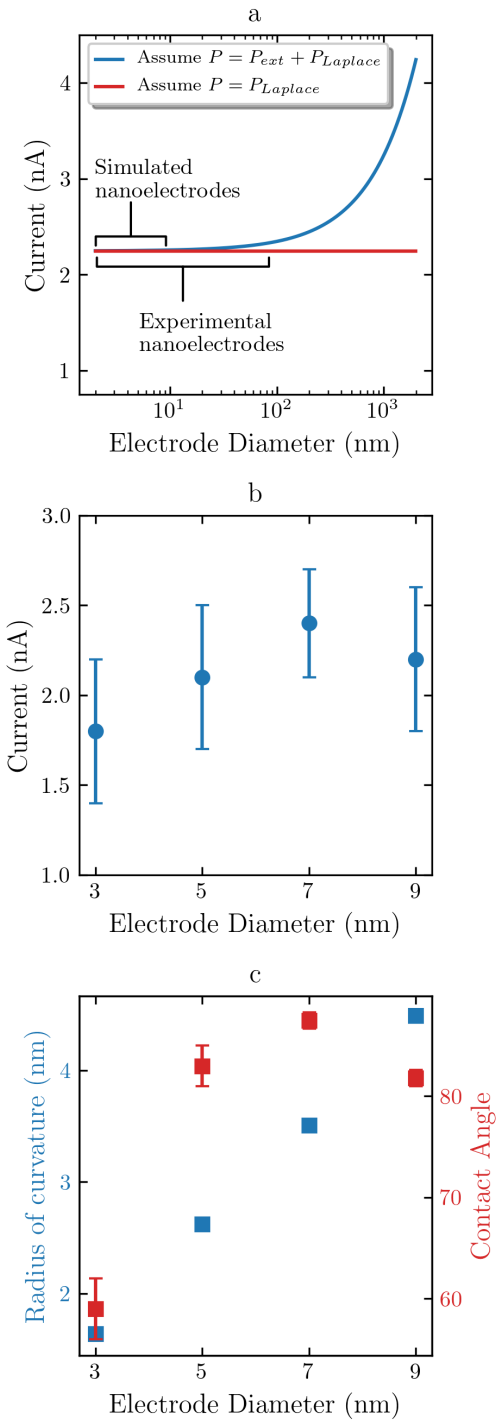

Figure 3. Effect of the diameter of the electrode on the stationary current and shape of the bubble. a) Residual currents as a function of electrode diameter predicted by the analytical model of eq. 1 (blue line) and its approximation in eq. 2 (red line), computed assuming a one-electron reaction, contact angle of 90°, P_{ext} = 1 atm, and adopting for K_H, D and σ the values for the models of water and gas.[44] (b) Residual current for the simulated 3, 5, 7 and 9 nm electrodes held at 200 mV. (c) Radii of curvature and contact angles for the simulated nanobubbles in stationary state for different electrode sizes. Discrepancies arise from variations in the surface energy that are, in turn, dependent on the mass density of the bubble and on the position of the three-phase line with respect to the electrode boundaries.

Equation 2 for the outflux of gas from the bubble should be valid beyond the steady state, regardless of the applied potential and whether there is electrochemical generation of gas. In particular, eq 2 should hold for the dissolution of nanobubbles in the absence of any applied potential. Hence, we test its predictive power through simulations of dissolution of nanobubbles of different sizes in the absence of a potential bias, recording the number N of particles in the nanobubble as a function of time. The diffusive particle outflux dN/dt is obtained from the simulations, averaging over 20 ns windows along the shrinking process. Dissolution simulations were carried out on three different electrodes of 3, 5, and 7 nm diameter (details provided in Supp. Info. D). The results, depicted in Figure 4a, confirm the independence of particle outflux with respect to size predicted by eq. 2: the slope of the curves is constant throughout the dynamics despite the fact that the bubble is shrinking, and the three electrodes exhibit the same slope.

Figure 4b compares: (i) the currents computed from the simulation of stationary states with applied potential, (ii) the outflux obtained from dissolution simulations without any potential, and (iii) the currents predicted by eq. 2 adopting for K_H, D and σ the values corresponding to the models of water and gas of the present study (see refs. [37, 43] and Supp. Info. B). Noticeably, Figure 4b confirms that the dissolution rate dN/dt is reliably predicted by eq. 2. However, the steady-state current under a low applied potential –the signature of the leaky regime- is larger than the one predicted by eq. 2, because a fraction of the produced gas leaks directly into the solution without going through the bubble. This leaked mass is not taken into account when assuming that the current is identical to the diffusive outflux, an approximation that is valid only for the *tight* regime. Figure 4 shows that at the higher potentials, when the contact angle is high and all gas generated by the electrochemical reaction enters the nanobubble, the steady-state currents match those predicted by the analytical model.

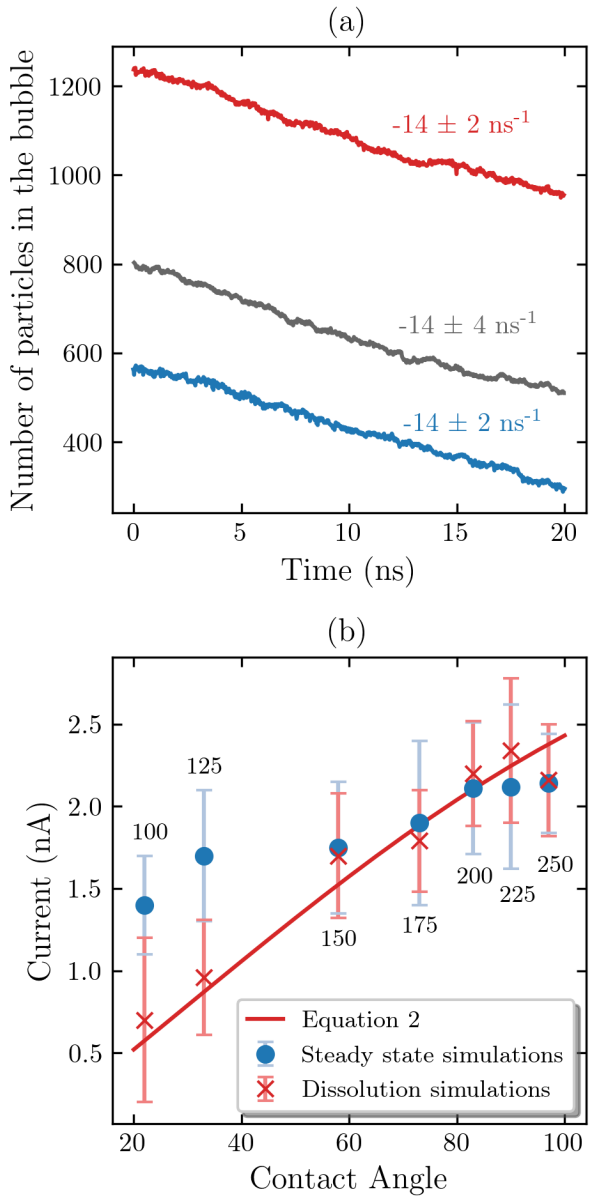

Figure 4. The analytical model quantitatively predicts the dissolution rates of bubbles and the stationary currents in the tight regime measured in the simulations. (a) Size of the nanobubble as a function of time during molecular simulations for the dissolution of nanobubbles in the absence of an applied potential (See Supp. Info. D). Blue, grey, and red curves correspond to simulations from electrodes of 3, 5, and 7 nm diameter respectively. Initial configurations were held at 200 mV. The numbers next to the curves indicate the slope obtained from block averages using 5 ns spans. (b) The red line shows the stationary currents on 5 nm electrodes covered by a nanobubble in the tight regime, as predicted by eq. 2. Blue circles show the residual currents obtained from stationary state molecular simulations. Numbers next to the data-points indicate the applied potential of each simulation in mV. Red crosses show the currents that correspond to the dissolution fluxes measured as the average number of moles of gas lost per unit time multiplied by Faraday's constant through dissolution simulations. The theoretical predictions assume gas solubility, s = 6.9 × 10^{-4} M, liquid-gas surface tension σ = 57 mJ/m^2 and diffusion coefficient D = 4.8 × 10^{-5} cm^2s^{-1} computed from simulations of mW water and gas model in refs. [37, 43] (see Supp. Info. B).

Maximization of the rates of gas-producing electrochemical reactions demands strategies to manage the catastrophic collapse of the current to small stationary values upon bubble nucleation. This study provides critical insights to optimize the design and operation conditions of electrochemical devices at a nanoscale level. As the reaction in the presence of a pinned bubble can only proceed at the perimeter of the electrode,[35-36] it may be expected that the miniaturization of electrocatalysts to the nanoscale would amplify the detrimental effect of bubble formation on reaction rates. At odds with that expectation, this study demonstrates that bubble-covered electrodes of diameter as small as 3 nm to as large as ~1 μm have stationary currents that are identical within the 1 nA uncertainty[35] of the experiments. Using an analytical model validated by simulations that combine kinetic Monte Carlo to model the potential dependence of the electrochemical reaction and molecular dynamics, we elucidate that the independence of the stationary current to the size of the electrode originates from the compensation of the growth in the area of the bubble and the decrease in its Laplace pressure with increasing electrode size. We demonstrate that this compensation is also at the heart of the impossibility to increase the stationary current by increasing the electrochemical potential. All together these results point to key advantages of using arrays of small nanoelectrodes, instead of a larger electrode of the same total area, to derive maximum current and conversion rate in gas-evolving reactions.

AUTHOR INFORMATION

Corresponding Authors

DAS: damian@qi.fcen.uba.ar; VM: valeria.molinero@utah.edu

ACKNOWLEDGEMENTS

This study was supported by the University of Utah through the Seed Grant "Molecular Modeling of Electrochemically Generated Nanobubbles" to VM, and the Agencia Nacional de Promoción Científica y Tecnológica de Argentina (ANPCyT) through PICT 2016-3167 to DAS. We thank the Center of High Performance Computing at The University of Utah for technical support and a grant of computing time.

Supporting Information Available:

The Supporting Information is available free of charge on the ACS Publications website. The pdf file contains sections that present: A) computational methods and force field parameters, B) gas concentration profiles before bubble formation, C) gas density profile of stationary bubbles, D) dissolution rates of nanobubbles, E) the dependence of the gas outflux on bubble geometry, F) caption of Supporting Movie S1. Movie S1: Side view of the evolution of an unpinned nanobubble under the conditions of Supporting Figure S5 (MPG).

REFERENCES

(1) Zhao, X.; Ren, H.; Luo, L. Gas Bubbles in Electrochemical Gas Evolution Reactions. *Langmuir* **2019,** *16*, 5392-5408.

(2) Roger, I.; Shipman, M. A.; Symes, M. D. Earth-Abundant Catalysts for Electrochemical and Photoelectrochemical Water Splitting. *Nat. Rev. Chem.* **2017,** *1*, 0003.

(3) Voiry, D.; Shin, H. S.; Loh, K. P.; Chhowalla, M. Low-Dimensional Catalysts for Hydrogen Evolution and CO2 Reduction. *Nat. Rev. Chem.* **2018,** *2*, 0105.

(4) Lu, Q.; Rosen, J.; Zhou, Y.; Hutchings, G. S.; Kimmel, Y. C.; Chen, J. G.; Jiao, F. A Selective and Efficient Electrocatalyst for Carbon Dioxide Reduction. *Nat. Commun.* **2014,** *5*, 3242.

(5) Li, Y.; Gao, W.; Ci, L.; Wang, C.; Ajayan, P. M. Catalytic Performance of Pt Nanoparticles on Reduced Graphene Oxide for Methanol Electro-Oxidation. *Carbon* **2010,** *48*, 1124-1130.

(6) Yang, J.; Cooper, J. K.; Toma, F. M.; Walczak, K. A.; Favaro, M.; Beeman, J. W.; Hess, L. H.; Wang, C.; Zhu, C.; Gul, S. A Multifunctional Biphasic Water Splitting Catalyst Tailored for Integration with High-Performance Semiconductor Photoanodes. *Nat. Mater.* **2017,** *16*, 335.

(7) Svetovoy, V. B.; Sanders, R. G.; Elwenspoek, M. C. Transient Nanobubbles in Short-Time Electrolysis. *J. Phys.: Condens. Matter* **2013,** *25*, 184002.

(8) Hao, R.; Fan, Y.; Howard, M. D.; Vaughan, J. C.; Zhang, B. Imaging Nanobubble Nucleation and Hydrogen Spillover During Electrocatalytic Water Splitting. *Proc, Natl. Acad. Sci. U. S. A.* **2018,** *115*, 5878-5883.

(9) Rees, N. V.; Compton, R. G. Sustainable Energy: A Review of Formic Acid Electrochemical Fuel Cells. *J. Solid State Electrochem.* **2011,** *15*, 2095-2100.

(10) Walter, M. G.; Warren, E. L.; McKone, J. R.; Boettcher, S. W.; Mi, Q.; Santori, E. A.; Lewis, N. S. Solar Water Splitting Cells. *Chem. Rev.* **2010,** *110*, 6446-6473.

(11) Mazloomi, S.; Sulaiman, N. Influencing Factors of Water Electrolysis Electrical Efficiency. *Renewable Sustainable Energy Rev.* **2012,** *16*, 4257-4263.

(12) Dapkus, K. V.; Sides, P. J. Nucleation of Electrolytically Evolved Hydrogen at an Ideally Smooth Electrode. *J. Colloid Interface Sci.* **1986,** *111*, 133-151.

(13) Mao, S.; Wen, Z.; Huang, T.; Hou, Y.; Chen, J. High-Performance Bi-Functional Electrocatalysts of 3D Crumpled Graphene–Cobalt Oxide Nanohybrids for Oxygen Reduction and Evolution Reactions. *Energy Environ. Sci.* **2014,** *7*, 609-616.

(14) Song, J.; Li, S.; Zhao, C.; Lu, Y.; Zhao, D.; Sun, J.; Roy, T.; Carmalt, C. J.; Deng, X.; Parkin, I. P. A Superhydrophilic Cement-Coated Mesh: An Acid, Alkali, and Organic Reagent-Free Material for Oil/Water Separation. *Nanoscale* **2018,** *10*, 1920-1929.

(15) Weijs, J. H.; Lohse, D. Why Surface Nanobubbles Live for Hours. *Phys. Rev. Lett.* **2013,** *110*, 054501.

(16) Hinnemann, B.; Moses, P. G.; Bonde, J.; Jørgensen, K. P.; Nielsen, J. H.; Horch, S.; Chorkendorff, I.; Nørskov, J. K. Biomimetic Hydrogen Evolution: MoS2 Nanoparticles as Catalyst for Hydrogen Evolution. *J. Am. Chem. Soc.* **2005,** *127*, 5308-5309.

(17) Gong, M.; Wang, D.-Y.; Chen, C.-C.; Hwang, B.-J.; Dai, H. A Mini Review on Nickel-Based Electrocatalysts for Alkaline Hydrogen Evolution Reaction. *Nano Res.* **2016,** *9*, 28-46.

(18) Wang, H.; Lu, Z.; Kong, D.; Sun, J.; Hymel, T. M.; Cui, Y. Electrochemical Tuning of Mos2 Nanoparticles on Three-Dimensional Substrate for Efficient Hydrogen Evolution. *ACS Nano* **2014,** *8*, 4940-4947.

(19) Su, H.; Fang, Y.; Chen, F.; Wang, W. Monitoring the Dynamic Photocatalytic Activity of Single Cds Nanoparticles by Lighting up H 2 Nanobubbles with Fluorescent Dyes. *Chem. Sci.* **2018,** *9*, 1448-1453.

(20) Li, S.; Du, Y.; He, T.; Shen, Y.; Bai, C.; Ning, F.; Hu, X.; Wang, W.; Xi, S.; Zhou, X. Nanobubbles: An Effective Way to Study Gas-Generating Catalysis on a Single Nanoparticle. *J. Am. Chem. Soc.* **2017,** *139*, 14277-14284.

(21) Chen, Q.; Ranaweera, R.; Luo, L. Hydrogen Bubble Formation at Hydrogen-Insertion Electrodes. *J. Phys. Chem. C* **2018,** *122*, 15421-15426.

(22) Edwards, M.; Robinson, D.; Ren, H.; Cheyne, C.; Tan, C.; White, H. S. Nanoscale Electrochemical Kinetics & Dynamics: The Challenges and Opportunities of Single-Entity Measurements. *Faraday Discuss.* **2018,** *210*, 9-28.

(23) Luo, L.; White, H. S. Electrogeneration of Single Nanobubbles at Sub-50-Nm-Radius Platinum Nanodisk Electrodes. *Langmuir* **2013,** *29*, 11169-11175.

(24) Chen, Q.; Luo, L.; Faraji, H.; Feldberg, S. W.; White, H. S. Electrochemical Measurements of Single H2 Nanobubble Nucleation and Stability at Pt Nanoelectrodes. *J. Chem. Phys. Lett.* **2014,** *5*, 3539-3544.

(25) Chen, Q.; Luo, L.; White, H. S. Electrochemical Generation of a Hydrogen Bubble at a Recessed Platinum Nanopore Electrode. *Langmuir* **2015,** *31*, 4573-4581.

(26) Chen, Q.; Wiedenroth, H. S.; German, S. R.; White, H. S. Electrochemical Nucleation of Stable N2 Nanobubbles at Pt Nanoelectrodes. *J. Am. Chem. Soc.* **2015,** *137*, 12064-12069.

(27) German, S. R.; Chen, Q.; Edwards, M. A.; White, H. S. Electrochemical Measurement of Hydrogen and Nitrogen Nanobubble Lifetimes at Pt Nanoelectrodes. *J. Electrochem. Soc.* **2016,** *163*, H3160-H3166.

(28) German, S. R.; Edwards, M. A.; Chen, Q.; Liu, Y.; Luo, L.; White, H. S. Electrochemistry of Single Nanobubbles. Estimating the Critical Size of Bubble-Forming Nuclei for Gas-Evolving Electrode Reactions. *Faraday Discuss.* **2016,** *193*, 223-240.

(29) German, S. R.; Edwards, M. A.; Chen, Q.; White, H. S. Laplace Pressure of Individual H2 Nanobubbles from Pressure–Addition Electrochemistry. *Nano Lett.* **2016,** *16*, 6691-6694.

(30) Ren, H.; German, S. R.; Edwards, M. A.; Chen, Q.; White, H. S. Electrochemical Generation of Individual O2 Nanobubbles Via H2O2 Oxidation. *J. Chem. Phys. Lett.* **2017,** *8*, 2450-2454.

(31) Moreno-Soto, Á.; German, S. R.; Ren, H.; Van Der Meer, D.; Lohse, D.; Edwards, M. A.; White, H. S. The Nucleation Rate of Single O2 Nanobubbles at Pt Nanoelectrodes. *Langmuir* **2018,** *34*, 7309–7318.

(32) German, S. R.; Edwards, M. A.; Ren, H.; White, H. S. Critical Nuclei Size, Rate, and Activation Energy of H2 Gas Nucleation. *J. Am. Chem. Soc.* **2018,** *140*, 4047-4053.

(33) Chen, Q.; Luo, L. Correlation between Gas Bubble Formation and Hydrogen Evolution Reaction Kinetics at Nanoelectrodes. *Langmuir* **2018,** *34*, 4554-4559.

(34) Lemay, S. G. Noise as Data: Nucleation of Electrochemically Generated Nanobubbles. *ACS nano* **2019,** *13*, 6141-6144.

(35) Liu, Y.; Edwards, M. A.; German, S. R.; Chen, Q.; White, H. S. The Dynamic Steady State of an Electrochemically Generated Nanobubble. *Langmuir* **2017,** *33*, 1845-1853.

(36) Perez Sirkin, Y. A.; Gadea, E. D.; Scherlis, D. A.; Molinero, V. Mechanisms of Nucleation and Stationary States of Electrochemically Generated Nanobubbles. *J. Am. Chem. Soc.* **2019,** *141*, 10801-10811.

(37) Molinero, V.; Moore, E. B. Water Modeled as an Intermediate Element between Carbon and Silicon. *J. Phys. Chem. B* **2009,** *113*, 4008-4016.

(38) Lohse, D.; Zhang, X. Pinning and Gas Oversaturation Imply Stable Single Surface Nanobubbles. *Phys. Rev. E* **2015,** *91*, 031003.

(39) Factorovich, M. H.; Molinero, V.; Scherlis, D. A. Vapor Pressure of Water Nanodroplets. *J. Am. Chem. Soc.* **2014**, 136, 4508-4514.

(40) Lohse, D.; Zhang, X. Surface Nanobubbles and Nanodroplets. *Rev. Mod. Phys.* **2015**, 87, 981-1035.

(41) Zhu, X.; Verzicco, R.; Zhang, X.; Lohse, D. Diffusive Interaction of Multiple Surface Nanobubbles: Shrinkage, Growth, and Coarsening. *Soft Matter* **2018**, 14, 2006-2014.

(42) Maheshwari, S.; Van Der Hoef, M.; Zhang, X.; Lohse, D. Stability of Surface Nanobubbles: A Molecular Dynamics Study. *Langmuir* **2016**, 32, 11116-11122.

(43) Jacobson, L. C.; Molinero, V. A Methane-Water Model for Coarse-Grained Simulations of Solutions and Clathrate Hydrates. *J. Phys. Chem. B* **2010,** *114*, 7302-7311.